Journal of Nuclear Materials 407 (2010) 16–28

Contents lists available at ScienceDirect

Journal of Nuclear Materials

journal homepage: www.elsevier.com/locate/jnucmat

Isochronal annealing of electron-irradiated dilute Fe alloys modelled by an *ab initio* based AKMC method: Influence of solute–interstitial cluster properties

R. Ngayam-Happy [a,b,c], P. Olsson [a,c], C.S. Becquart [b,c,*], C. Domain [a,b,c]

[a] EDF-R&D, Département Matériaux et Mécanique des Composants (MMC), Les Renardières, F-77818 Moret sur Loing Cedex, France
[b] Unité Matériaux et Transformations (UMET), UMR CNRS 8207, Université de Lille 1, ENSCL, F-59655 Villeneuve d'Ascq Cedex, France
[c] Laboratoire commun EDF-CNRS Etude et Modélisation des Microstructures pour le Vieillissement des Matériaux (EM2VM), France

A B S T R A C T

The evolution of the microstructure of dilute Fe alloys under irradiation has been modelled using a multiscale approach based on *ab initio* and atomistic kinetic Monte Carlo simulations. In these simulations, both self interstitials and vacancies, isolated or in clusters, are considered. Isochronal annealing after electron irradiation experiments have been simulated in pure Fe, Fe–Cu and Fe–Mn dilute alloys, focusing on recovery stages I and II. The parameters regarding the self interstitial – solute atom interactions are based on *ab initio* predictions and some of these interactions have been slightly adjusted, without modifying the interaction character, on isochronal annealing experimental data. The different recovery peaks are globally well reproduced. These simulations allow interpreting the different recovery peaks as well as the effect of varying solute concentration. For some peaks, these simulations have allowed to revisit and re-interpret the experimental data. In Fe–Cu, the trapping of self interstitials by Cu atoms allows experimental results to be reproduced, although no mixed dumbbells are formed, contrary to the former interpretations. Whereas, in Fe–Mn, the favorable formation of mixed dumbbell plays an important role in the Mn effect.

1. Introduction

In nuclear power plants, reactor materials may undergo degradation in physical and mechanical properties due to severe in-service irradiation. However, understanding how microstructures and thus the mechanical properties evolve under irradiation is a challenging task as the materials are maintained in nonequilibrium conditions, for which the existing theoretical frameworks are not yet fully established as the situations are very complex. In particular, in the irradiated pressure vessel steels, weakly alloyed, the formation of clusters enriched in Cu, Ni, Mn and Si [1,2] under neutron irradiation is an intriguing phenomenon with significant consequences in terms of the observed hardening.

To tackle this problem, we use an Atomic Kinetic Monte Carlo (AKMC) model based on the diffusion of point defects. Its aim is to simulate the medium term formation of the Cu–Ni–Mn–Si enriched clusters under irradiation. The model has as a first step been parameterized on thermal ageing experiments of alloys of growing complexity [3,4]. This first step insured that the interactions between vacancies and solute atoms were correctly treated. As a second step, we introduce interstitials in the model and here present the procedure adopted to assess the validity of the AKMC parameters related to these interstitials. The method consists in the simulation of isochronal annealing of dilute Fe model alloys for which detailed experiments exist as points of comparison.

In the first part, the AKMC model is presented. The second part recalls the basic ingredients of isochronal annealing experiments. In the third part, the AKMC modelling of recovery experiments are presented for Fe, dilute Fe–Cu then dilute Fe–Mn alloys. Based on these results, we then discuss the validity of the model and the possible reinterpretations of the experimental results from the literature.

2. The Monte Carlo model

The Monte Carlo code, LAKIMOCA, developed at EDF [5], has been improved to treat complex alloys (Fe–CuNiMnSi) as well as interstitials that are introduced in a large amount during irradiation [6]. The motive for introducing interstitials in the vacancy AKMC was twofold: first of all, interstitials, formed under irradiation, move very quickly and can recombine with vacancies, decreasing the amount of vacancies available for diffusion. Second, solute atoms interact with interstitials, e.g. *ab initio* results indicate that Mn is very likely to be able to diffuse via mechanisms involving interstitials [7] as well as vacancies, while the other solutes (Cu, Ni and Si), which establish strong bonds with vacancies, are more likely to diffuse via vacancies only [8]. Previous calculations [7] indicate that even when a solute lies in the vicinity of a dumbbell,

* Corresponding author.
E-mail address: charlotte.becquart@univ-lille1.fr (C.S. Becquart).

0022-3115/$ - see front matter © 2010 Elsevier B.V. All rights reserved.
doi:10.1016/j.jnucmat.2010.07.004

the dumbbell remains oriented along the ⟨1 1 0⟩ direction. Thus, only ⟨1 1 0⟩ dumbbells are treated in our code.

The model is based on the residence time algorithm [9]. Both vacancy and interstitial diffusion is determined by the calculation of the probabilities to jump to a first nearest neighbour site. This probability is obtained for each solute atom X as follows:

$$\Gamma_X = \nu \exp\left(-\frac{E_a^X}{kT}\right) \quad (1)$$

where ν is the attempt frequency, chosen equal to $6 \times 10^{12}\ s^{-1}$ (a value close to the atomic vibration frequency of $1 \times 10^{13}\ s^{-1}$), and E_a^X is the activation energy of the jump.

The activation energy E_a^X is obtained using an environment-dependent model, which satisfies the detailed balance rule:

$$E_a^X = E_a^0 + \frac{E_f - E_i}{2} \quad (2)$$

where E_i and E_f are the system energies, respectively, before and after the jump of the vacancy or of the interstitial. Recombination between an interstitial and a vacancy takes place as soon as they become second nearest neighbours.

The reference activation energy E_a^0 depends only on the type of the migrating atom: it is equal to

- the *ab initio* vacancy migration energy in pure Fe when a vacancy jumps towards an Fe atom (0.62 eV);
- the *ab initio* solute migration energy in pure Fe when a vacancy jumps towards a solute atom (0.54 eV for Cu and 1.03 eV for Mn);
- the *ab initio* migration-60° rotation energy of the migrating atom in pure Fe when a dumbbell migrates (0.31 eV).

E_i and E_f are determined using pair interactions, according to the following equation:

$$E = \sum_{i=1,2} \sum_{j<k} \varepsilon^{(i)}(S_j - S_k) + E_{\text{dumb}} \quad (3)$$

where i equals 1 or 2 and corresponds respectively to first or second nearest neighbour interactions, j and k to the lattice sites and S_j (resp. S_k) is the species occupying site j (resp. k): S_j in {X, V} where X = Fe, Cu, or Mn.

When the mobile element is a vacancy, the interactions due to the interstitials are not taken into account, and E_{dumb} is taken as 0. When an interstitial jumps,

$$E_{\text{dumb}} = N_{\text{dumb}} E_{\text{for}}^{\langle 110\rangle} + \sum_{\text{dumb}_i} \begin{pmatrix} \sum_j E_b^{1\text{nnComp}}(X^{\text{dumb}_i} - X_j^{1\text{nncomp}}) + \sum_j E_b^{1\text{nnTens}}(\text{dumb}_{\text{Fe-Fe}} - X_j^{1\text{nnTens}}) \\ E_b^{\text{mixed}}(X^{\text{dumb}_i} - Y^{\text{dumb}_i}) + \sum_{j<i} E_b(\text{dumb}_i - \text{dumb}_j) \end{pmatrix} \quad (4)$$

where X_i, X_j et X_k can be Fe, Cu, or Mn. $E_{\text{for}}^{\langle 110\rangle}$ is the ⟨1 1 0⟩ dumbbell formation energy in pure Fe. The meaning of the terms in Eq. (4) is represented in Fig. 1.

The interactions between two dumbbells E_b(dumb–dumb) are taken into account for 1st and 2nd nearest neighbours and are considered identical whatever the dumbbell orientation is. This choice in the AKMC model is motivated by the fact that nor our *ab initio* calculations, nor literature results on interstitial clusters have revealed a clear influence of dumbbell orientation on the binding energy. The interaction values are chosen to be 0.7 eV and 0.48 eV when the two dumbbells are 1st or 2nd nearest neighbours, respectively. We assume furthermore that the type of the two dumbbells (⟨1 1 0⟩$_{\text{Fe-Fe}}$ or mixed ⟨1 1 0⟩$_{\text{Fe-X}}$ dumbbells) does not influence either 1st or 2nd nearest neighbour interaction values. In the KMC model, the migration of the di-interstitial, described in Fig. 2, is achieved by successive jumps of the two dumbbells, which go through a configuration where they are 2nd nearest neighbours. These considerations about di-interstitial interaction and migration do not mean that, in the model, a di-interstitial containing ⟨1 1 0⟩$_{\text{Fe-X}}$ mixed dumbbells migrates with the same energy as a di-interstitial containing only ⟨1 1 0⟩$_{\text{Fe-Fe}}$ dumbbells. Fig. 2 and Eq. (2) indicate that a difference in activation energies would arise from the term E_a^0 even if the cohesive term $\frac{E_f - E_i}{2}$ is the same in both cases. With the interaction data described above and using Eq. (2), the activation barrier to overcome is 0.41 eV, which is in good agreement with the *ab initio* barrier calculated by Fu et al. (0.42 eV) [10]. Moreover with this model for interstitials, interstitial clusters of size ranging from three to six are also mobile.

The pair interactions $\varepsilon^{(i)}(S_j - S_k)$ necessary to determine E_i and E_f, have been obtained using a set of equations relating properties such as mixing, cohesive, surface energies and so on, that take into account first and second neighbour pair interactions. The energies used in this set of equations have been determined using *ab initio* calculations [4,7,8,11]. However, because *ab initio* calculations do have limitations and uncertainties, the *ab initio* values used in the parameterisation were compared to experiments or thermodynamical data, when they were available, and sometimes readjusted accordingly. This adjustment was made by simulating age hardening of binaries, ternaries and more complex alloys and comparing the obtained results with experimental ones. A detailed description of the parameterisation of the Fe–Cu system can be found in [12]. During this procedure some of the values obtained *ab initio* had to be slightly modified so as to obtain a set of values more in agreement with experiments and phase diagrams as well as with other *ab initio* data. The energy difference between the original *ab initio* data and the adjusted data was less than 0.1 eV which corresponds roughly to the *ab initio* uncertainty. The final values of the pair interaction parameters $\varepsilon^{(i)}(S_j - S_k)$ after the adjustments can be found in [6]. In [6], the data related to the motion of the SIA, thus used to determine E_{dumb} in Eq. (4), were *ab initio* data (no adjustment of these data has been made).

In the next paragraph, we present the procedure adopted to check the validity of these parameters, which consists in the simulation of isochronal annealing experiments of dilute Fe model alloys.

3. Isochronal annealing experiments of pure Fe and dilute Fe model alloys

In this kind of experiments, the materials are first irradiated at very low temperatures. Most of the time, the irradiations carried out are electronic, limiting the damage to simple Frenkel Pairs (FP). The irradiated materials are then isochronally annealed at a specific rate and their recovery is analysed either by electrical resistivity, magnetic after-effect or internal friction measurements.

In the case of pure Fe, the recovery experiments of Takaki et al. [13] are often cited as reference. The authors analysed by electrical resistivity the recovery of high-purity electron-irradiated Fe with irradiation doses ranging from 5.6×10^{-11} to $588.9 \times 10^{-11}\ \Omega\,m$, corresponding to doses close to $2\text{–}200 \times 10^{-6}$ in displacements per atom (dpa).

For dilute binary Fe alloys, Maury et al. [14–16] electron-irradiated Fe–X (X = Cu, Ni, Mn and Si) binary alloys that they analysed by electrical resistivity measurements. Abe and Kuramoto [17] made the same experiments for the Fe–Si binary alloys. Hasiguti [18] neutron-irradiated Fe–Ni binary alloys and analysed them using internal friction techniques. Blythe et al. [19] electron and/or neutron-irradiated Fe–X (X = Cu, Mn, Ni, Si, Co, and Au) binary alloys that were examined by magnetic after-effect measurements.

In the present work, we demonstrate the validity of the *ab initio* based KMC model by simulating recovery experiments of Fe, Fe–Cu

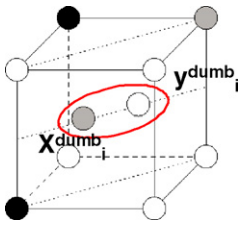

$E_b^{mixed}(X^{dumb_i} - Y^{dumb_i})$

Binding energy of a mixed dumbbell

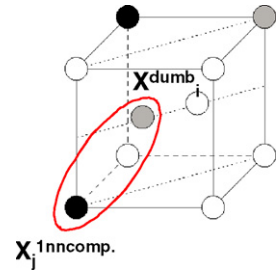

$E_b^{1nnComp}(X^{dumb_i} - X_j^{1nncomp.})$

Binding energy of the dumbbell with an atom positioned in the plane containing the dumbbell (compressive position). The type of the dumbbell atom the closest to the atom in the matrix is taken into account.

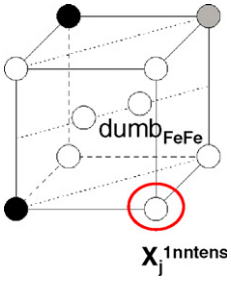

$E_b^{1nnTens}(X_j^{1nntens.} - dumb_{FeFe})$

Binding energy of the dumbbell with an atom positioned in the plane perpendicular to the dumbbell (tensile position).The dumbbell is considered as being a pure Fe dumbbell, only the type of solute in the tensile position is taken into account.

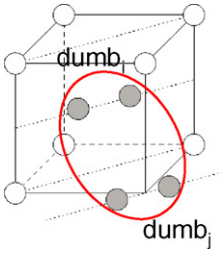

$E_b(dumb_i - dumb_j)$

Binding energy between two dumbbells. The interaction depends only on the separation distance between the two dumbbells. The interaction values are chosen to be 0.7 or 0.48 eV when the two dumbbells are respectively 1st or 2nd nearest neighbours

Fig. 1. Schematic description of the interaction terms taken into account in the activation energy determination when the moving object is a dumbbell.

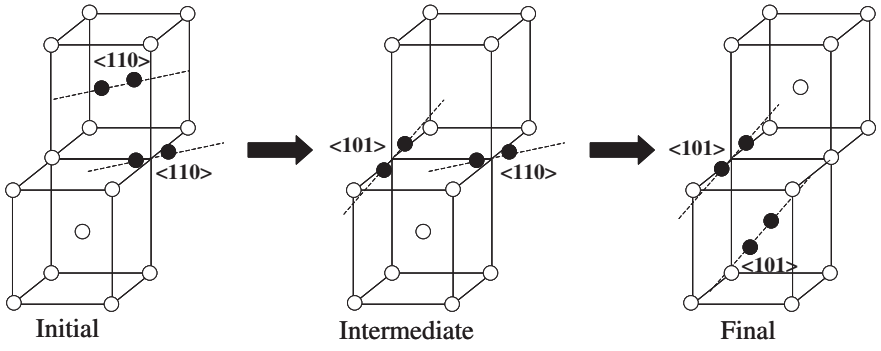

Fig. 2. Schematic representation of the migration path of a di-SIA in the KMC model by successive jumps of the two dumbbells. The di-SIA passes through an intermediate configuration for which the two dumbbells are 2nd nearest neighbours.

and Fe–Mn dilute alloys. The experimental results of Takaki et al. [13] have been used to investigate the model for pure Fe. For the Fe–Cu and Fe–Mn model alloys, we have used the results of Maury et al. [14,15]. These authors irradiated with 3 MeV electrons six dilute Fe–Mn model alloys (with compositions ranging from 0.01 at.% Mn to 3 at.% Mn) as well as four dilute Fe–Cu alloys (with compositions ranging from 0.005 at.% Cu to 0.04 at.% Cu). They analysed the recovery of the materials by electrical resistivity.

During isochronal annealing experiments, the pertinent property is the evolution of the differential isochronal resistivity recovery $-\frac{d}{dT}(\frac{\Delta\rho}{\Delta\rho_0})$ (with $\Delta\rho$ the difference $\rho - \rho_0$ between the resistivity measured at a given temperature and the residual resistivity of the material and $\Delta\rho_0$ the difference between the measured resistivity after irradiation and the residual resistivity) versus temperature. The spectra obtained exhibit a certain number of peaks, which can be associated with several processes, implicating the different point defects and their clusters. As the SIA migration energy is much lower than the vacancy migration energy, the events taking place at low temperatures (below 200 K) are associated with events involving only interstitial-type defects and their clusters.

These events have been classified into two main stages: stage I which, for pure Fe, ranges from 20 to 150 K, and stage II, which covers the range from 150 to 200 K. Fig. 3 represents the isochronal annealing spectra of pure Fe. In this figure, both KMC simulated spectra (in full lines and solid symbols) and Takaki et al. [13] experimental data (in dashed lines and open symbols) for two different doses are presented. An examination of the experimental spectra indicates that stage I consists of several peaks, three of which are relevant: I_{D1}, I_{D2} and I_E. The I_{D1} and I_{D2} peaks are experimentally observed at 101 and 108 K. They are attributed by the authors to close-pair recovery and to the correlated recombination of FP, respectively (SIAs and vacancies from the same FP). This event thus takes place after a short-range migration of the SIA. The I_E peak position ranges from 123 K for the highest dose (2.36×10^{-4} dpa) to 135 K for the lowest dose (4.27×10^{-5} dpa). This peak corresponds to the uncorrelated recombination of FP due to long-range migration of SIAs that generally recombine with a vacancy from another FP. Stage II consists of a single peak, denoted II, which, because it is also dose dependent, can be observed in a temperature range from 164 K (highest dose) to 175 K (lowest dose). Peak II is attributed to the migration of di-SIAs that are formed during the long-range migration of SIAs. In the case of dilute alloys, stage II may reveal several other peaks than the peak II of pure Fe. These peaks are generally related to processes due to the presence of solute atoms.

4. Kinetic Monte Carlo simulations of recovery experiments

The KMC simulations start by introducing a fixed number of FP in a 7.9×10^4 nm^3 box ($150 \times 150 \times 150$ bcc lattice units) with periodic boundary conditions applied in all directions. This step is equivalent to the experimental irradiation step, and the initial irradiation damage depends on the number of FP introduced.

To take into account the space correlation between the *V* and SIA of a given FP produced by a single electron (I_{D2} peak), the two elements are introduced in the simulation box within a certain distance range from each other. Furthermore, because there are no close-pairs introduced in the simulation box, the recovery stages from 0 K to I_{D1} due to close-pair recombination do not appear in the simulated spectra. We found that by choosing a distance between 3 and 6 Å, the characteristics of the defect population recovery for both close-pairs and correlated FP are well reproduced, i.e., the total recovery at the end of the simulated I_D peak falls in the 50–70% recovery range observed experimentally at the end of the I_{D2} peak.

All the isochronal annealing simulations have been carried out by increasing the temperature by steps of 3 K every 300 s. As the evolution of the electrical resistivity is correlated to the evolution of the defect population, the recovery has been analysed by following the evolution of all point defect populations and their clusters. In this scheme, we assume that each point defect (isolated or in cluster) has the same contribution to the electrical resistivity. Therefore the experimental differential isochronal resistivity recovery, $-\frac{d}{dT}(\frac{\Delta\rho}{\Delta\rho_0})$, has been replaced for the simulated spectra by the differential isochronal recovery of the total number of defects introduced in the simulation boxes, i.e., $-\frac{d}{dT}(\frac{n}{n_0})$, where n is the total number of FP remaining in the simulation box at a given temperature and n_0 is the initial number of FP introduced in the box.

The derivative at each temperature of the number of defects was obtained using a sliding average in order to smooth out possible short-term fluctuations with a constant subset size of four temperature steps (±6 K). Finally, all the simulated spectra presented

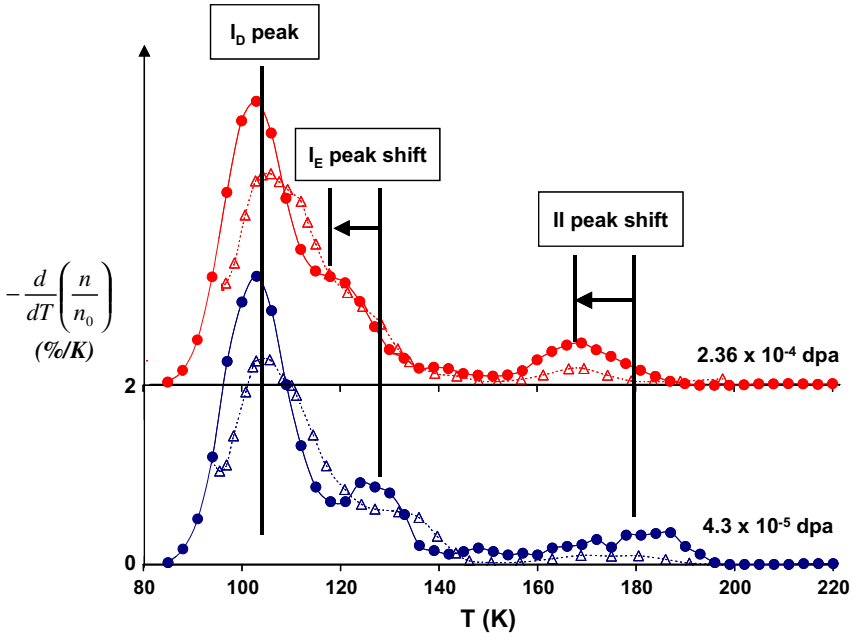

Fig. 3. Differential isochronal recovery spectra of pure Fe: influence of irradiation dose. The simulated results (full lines and solid symbols) were obtained for $150 \times 150 \times 150$ (in lattice units) simulation boxes, irradiated at 4.3×10^{-5} dpa (290 FP in the simulation box) and 2.36×10^{-4} dpa (1593 FP in the simulation box), which were then isochronally annealed at a rate of 3 K/300 s. For comparison, the corresponding experimental results (dashed lines and open symbols) of Takaki et al. [13], obtained for identical annealing conditions and dose, are also shown.

in the next sections are averaged spectra on three different simulations obtained with different random seeds. We have investigated the statistical error arising from the use of only three seeds and the results have shown that this consideration is enough to cancel statistical disturbances since the error generated with three and a higher number of replicas (between 4 and 10) lies between 0% and 6%.

4.1. AKMC recovery in pure Fe

This section presents the AKMC simulation recovery results obtained in pure Fe. Their consistency has been investigated in several steps. After the correct reproduction of the experimental stages was checked, a qualitative and quantitative analysis of the results was carried out, followed by a study of dose effect.

The simulated isochronal recovery spectra displayed in Fig. 3 exhibit three distinct stages with the same features as the experimentally observed I_D, I_E, and II stages described above. Moreover, as demonstrated in Fig. 4, the evolution of the different populations of point defects at each stage is in good agreement with Takaki and co-workers [13] interpretation of the corresponding experimental data.

The I_D peak appears in the simulated spectra for both doses around 105 K, 2.5 K below the experimental I_{D2} peak and is due to correlated recombinations of FP. A corresponding recovery of ~55% of the initial number of FP is observed in simulated spectra at the end of stage I_D. On the highest dose spectrum, the peak observed at 121 K (against 123 K experimentally) is the I_E peak which is due to the migration of SIAs, as shown in Fig. 4. This temperature difference is more pronounced for the lowest dose case, as the simulated I_E peak is observed 6 K below the experimental peak. This observation may suggest that there is an increasing quantitative limitation of the AKMC model with decreasing dose in reproducing the temperature of appearance of I_E peak. This can be due to the fact that very low doses imply introducing a very small amount of FP in the simulation box, which may be nonrepresentative to simulate an isochronal annealing experiment. However for the dose range of Fig. 3 this discrepancy still remains very low. The good agreement observed for peaks I_D and I_E has been obtained by lowering the *ab initio* value of the SIA migration energy from 0.37 eV to 0.31 eV, which agrees not only with the value deduced by the authors from the experimental spectra (0.27 ± 0.04 eV), but also with the results of *ab initio* calculations [10,20]. The last peak, which appears around 165 K for the highest dose case, corresponds to the peak II experimentally observed by Takaki and co-workers at 164 K. It is indeed due to the di-SIAs, formed during the long-range migration of SIAs, that migrate with an activation energy of 0.41 eV.

Another quantitative dissimilarity between simulated and experimental results is about the amplitude of I_D, I_E, and II peaks which appears generally to be higher for the simulated spectra than the experimental ones. This may come from the assumption we have made by equating electrical resistivity and defect populations. As we have demonstrated, this assumption is certainly worth it, since we have been able to reproduce qualitatively all the characteristics of experimental peaks. However, neglecting all the other contributions to electrical resistivity has probably led to an over estimation of the recovery.

A little shoulder can be observed in the simulated spectra at the end of the I_E peak. This peak is due to the migration of tri-SIAs formed during stage I_E (Fig. 4), since they have the same activation energy as the SIAs in our AKMC model.

The AKMC model for pure Fe was further validated by investigating the dose effect on the isochronal annealing spectra as this study is available in [13]. The experiments indicate that no modifications of the I_D peaks appear with the dose; these peaks are thus dose-independent. Contrary to the I_D peaks, the I_E and II peaks are dose dependent and shift towards lower temperatures when the irradiation dose increases. As can be seen in Fig. 3, the dose effect is correctly reproduced, since the experimentally observed shifts of the I_E and II peaks and absence of dose dependence for the I_D peak have also been observed on simulated spectra.

4.2. AKMC recovery of dilute Fe–Cu alloys

The experimental [15] and simulated spectra of the evolution with temperature of the differential isochronal recovery in dilute Fe–Cu alloys are represented in Figs. 5a and 5b. Both results were obtained in pure Fe and alloys isochronally annealed at a rate of 3 K/300 s after being initially irradiated at a dose of 4.2×10^{-5} dpa. The consistency of the KMC results was studied by checking for the reproduction of experimental peaks, the effect of the addition of Cu, and the qualitative and quantitative worth of these results.

4.2.1. Stage I

The experimental spectra indicate that the addition of Cu up to 0.04 at.% has no influence on I_D peaks whose amplitude and position do not change. This issue is also well reproduced by the spectra obtained in KMC simulations. The most significant effect of the addition of Cu experimentally observed in stage I is the gradual

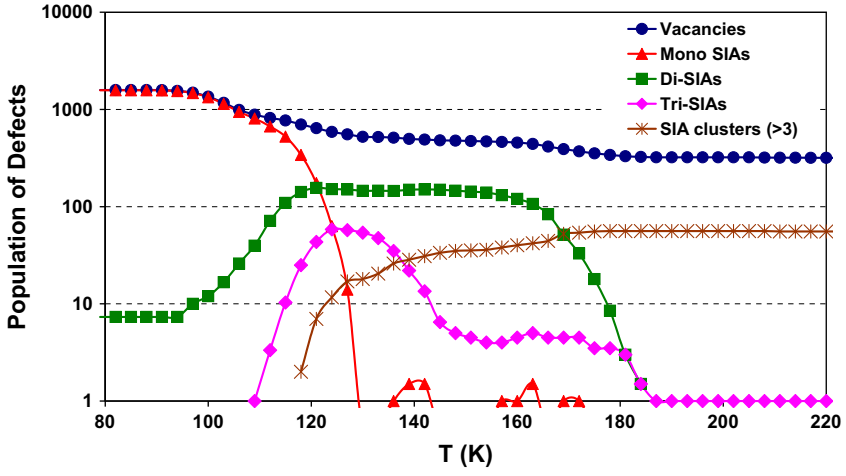

Fig. 4. Defect population evolution with annealing temperature for pure Fe isochronally annealed at a rate of 3 K/300 s after being electron-irradiated at 2.36×10^{-4} dpa.

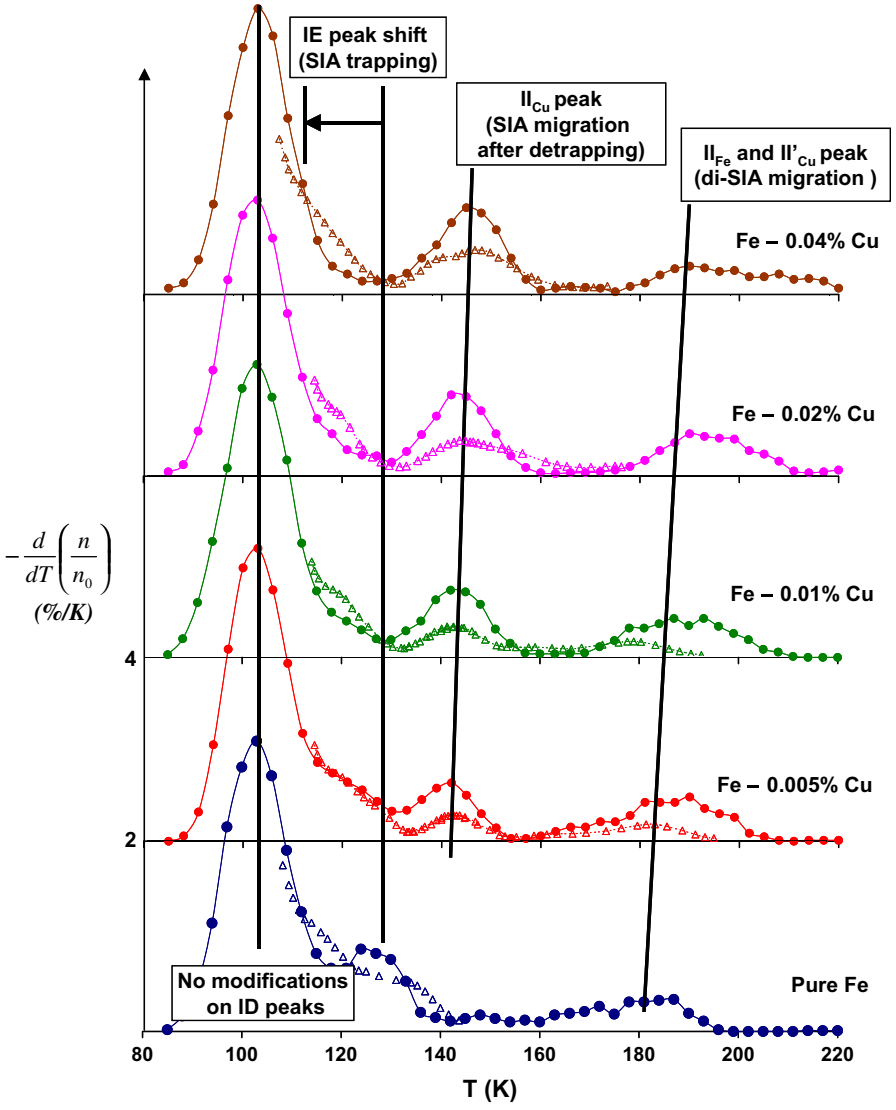

Fig. 5a. Differential isochronal recovery spectra of Fe and Fe–Cu alloys: influence of Cu content. The simulated results (full lines and solid symbols) were obtained for $150 \times 150 \times 150$ (in lattice units) simulation boxes, initially containing 284 FP (corresponding to an initial irradiation dose of 4.2×10^{-5} dpa), which were isochronally annealed at a rate of 3 K/300 s. For comparison, experimental results (dashed lines and open symbols) of Maury et al. [15], obtained for identical conditions, are also shown.

suppression of the I_E peak with increasing concentration of solute atoms. According to Maury and co-workers, this disappearance of peak I_E is due to an efficient trapping of SIAs by the Cu atoms. The set of *ab initio* data used to parameterise the KMC model indicates that a Cu atom in a tensile position can indeed trap a $\langle 1\,1\,0\rangle_{Fe-Fe}$ dumbbell [21]. Moreover, the study of the evolution of the population of SIAs with annealing temperature (Fig. 6) clearly shows an increasing amount of trapped SIAs with increasing Cu concentration in the temperature range of peak I_E. The KMC results confirm therefore the explanation of Maury and co-workers to account for the suppression of the I_E peak. Note that a slight increase in the value of $X1nn^{Tens}\_\langle 1\,1\,0\rangle_{Fe-Fe}$ (from the *ab initio* value of 0.07 eV to the adjusted value of 0.13 eV, see Table 1) is enough to obtain a good agreement between the simulated and experimental spectra.

Although the main features of stage I are qualitatively well reproduced by the model, two quantitative differences with the experimental results have to be mentioned. In pure Fe first of all, a 8 K shift from the experimental position is observed for the simulated I_E peak. This peculiarity, due to some AKMC limitations at very low doses, has been commented on previously in the pure Fe section. Second of all, with increasing amount of Cu, the suppression of I_E peak is more marked on the simulated spectra. It is not obvious to give an accurate explanation of this effect since it may originate from a combination of different sources of errors including for instance an over estimation of the trapping efficiency of Cu in these alloys, the neglect in the model of other contributions to the isochronal recovery, the statistical distribution of Cu atoms in the simulation box, or other complex cases.

4.2.2. Stage II

According to Maury and co-workers, the suppression of the I_E peak is followed by the appearance of two new peaks labelled II_{Cu} for the peak around 145 K, and II'_{Cu} for the one around 160 K. The authors have also observed the appearance of a peak situated between 170 and 200 K, which they attributed to residual impurities.

With increasing concentration of Cu in the alloy, the II_{Cu} peak shifts slightly towards higher temperatures and its amplitude increases. According to Maury and co-workers, this behaviour, typical of de-trapping, is due to the migration of the SIAs previously trapped. The KMC spectra also show a peak with the same features, and a close analysis of the SIAs population results in an interpreta-

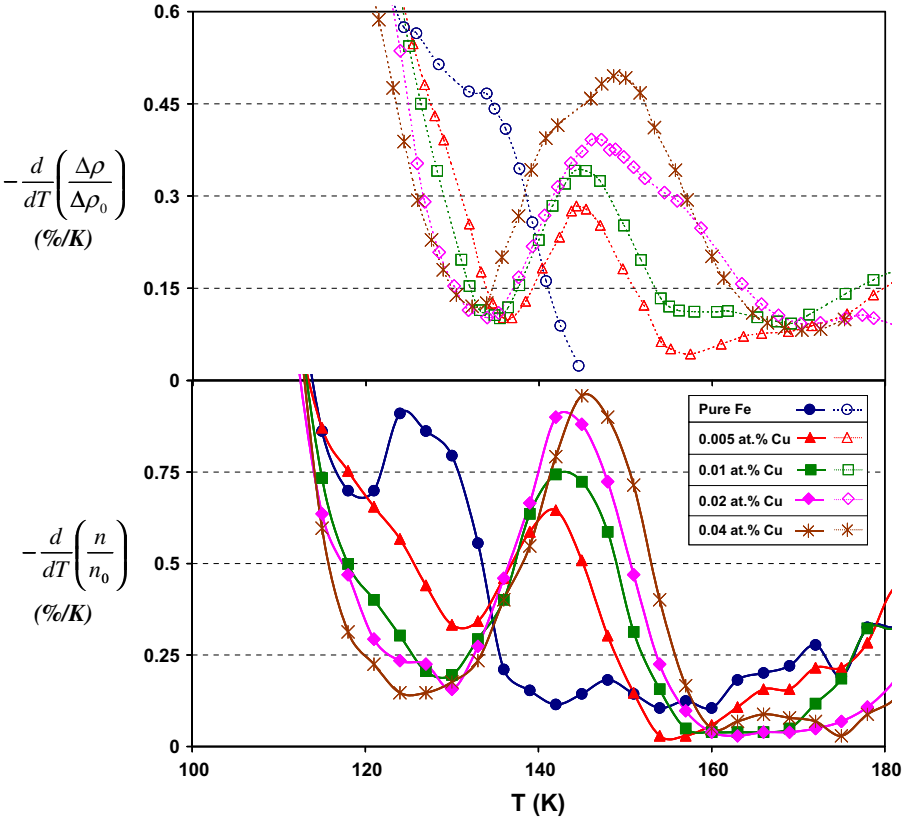

Fig. 5b. Zoom of Fig. 5a.

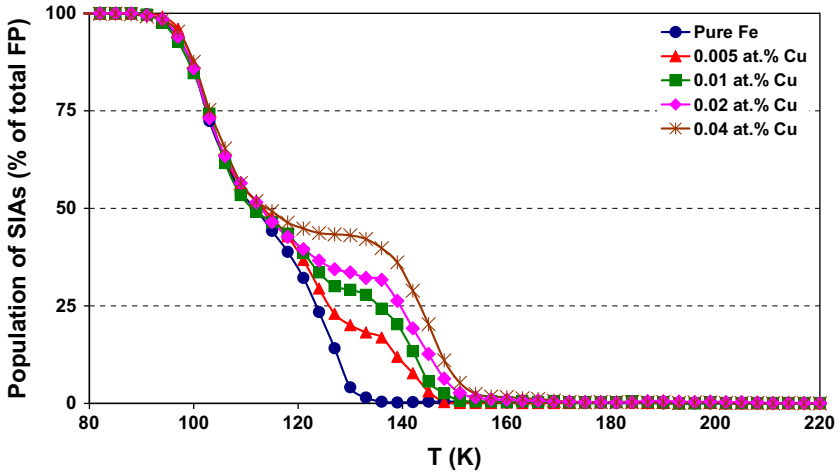

Fig. 6. SIA population evolution with temperature for pure Fe and Fe–Cu alloys isochronally annealed at a rate of 3 K/300 s after being electron-irradiated at 4.2×10^{-5} dpa. The results are represented in percentage of the 284 FP initially introduced in the simulation box.

tion in agreement with experiment. Moreover, an attempt to build a more refined explanation of the behaviour of this peak can be done, based on the results provided by the KMC simulations. Indeed, the simulations indicate that an increasing amount of trapped SIAs is enough to account for this behaviour. As the amplitude of a peak is related to the amount of defects recovered, it appears straightforward that the alloy with the greatest concentration of de-trapped SIAs would have the highest amplitude, which is what is observed for both experimental and simulated recovery spectra. The shift of the II_{Cu} peak to higher temperatures can be attributed to an increasing "effective" de-trapping energy with increasing concentration of trapped SIAs, even if the de-trapping process is activated at the same temperature for all the alloys.

Concerning the II'_{Cu} peak observed by Maury and co-workers, the evolution of its height is similar to that of II_{Cu}, but contrary to II_{Cu}, this peak shifts to low temperatures when the Cu content increases. According to these authors, this behaviour is characteristic of the migration of mixed Fe–Cu dumbbells that have formed during stage I_E. However, *ab initio* calculations do not predict the formation of stable mixed dumbbells in dilute Fe–Cu alloys [21], therefore we propose a different explanation for the events occurring in the temperature range after stage II_{Cu}.

Table 1
Summary of the changes in the energies used to calculate E_{dumb} (Eq. (4)). The *ab initio* calculations were performed within density functional theory using ultra soft pseudo-potentials and the Generalized Gradient Approximation approach with the VASP code [6].

		Cu		Mn	
		Ab initio value (eV)	Adjusted value (eV)	*Ab initio* value (eV)	Adjusted value (eV)
$E^{mig}_{\langle 110\rangle_{Fe-X}}$		0.32	–	0.34	0.38
$E^{bind}_{\langle 110\rangle_{Fe-X}}$	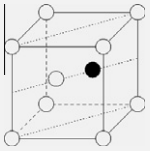	−0.46	–	0.37	0.39
$E^{bind}_{\langle 110\rangle_{X-X}}$	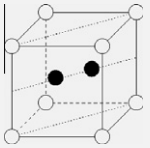	−0.36	–	0.47	0.41
$X1nn^{Tens}\_\langle 1\,1\,0\rangle_{Fe-Fe}$	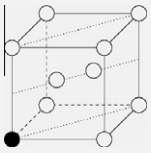	0.07	0.13	−0.36	–
$X1nn^{Comp}\_\langle 1\,1\,0\rangle_{Fe-Fe}$	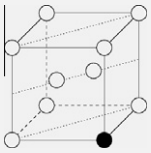	−0.01	–	0.10	0.02
$X1nn^{Comp}\_\langle 1\,1\,0\rangle_{Fe-X}$	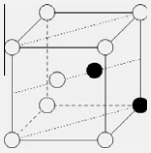	−0.28	–	−0.08	–

First of all, if we assume like Maury that the peaks observed between 170 and 200 K are due to residual impurities, the relevance of any smaller peak, like II'_{Cu} would be dubious. Moreover, because such a peak has not been clearly identified in the simulated spectra, we think that the most important feature, common to both simulated and experimental spectra, is the remarkable asymmetry observed for the II_{Cu} peak as the Cu concentration increases (shift of the right part of the peak to higher temperature as observed in Fig. 5b). This is due to a "temporary" re-trapping process of the migrating SIAs as they can still encounter Cu atoms. This phenomenon would then be more pronounced for the alloy with the highest Cu concentration, which is what is observed. The term temporary is used here because the re-trapping process should rather be considered as a slowing-down process for the migrating SIAs, as the temperature is enough to overcome the trapping of Cu atoms.

Second, the simulated spectra point out the formation of recovery peaks in the temperature range of the peaks Maury et al. attributed to residual impurities. On the basis of the simulated results,

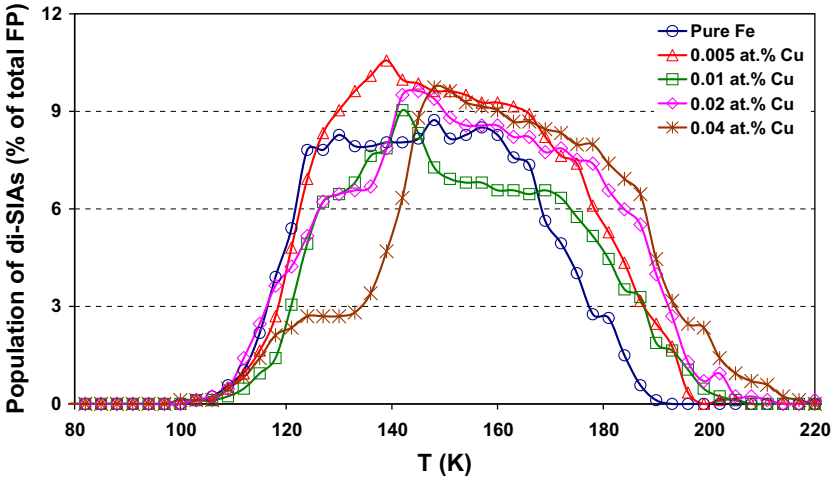

Fig. 7. Di-SIA population evolution with temperature for pure Fe and Fe–Cu alloys isochronally annealed at a rate of 3 K/300 s after being electron-irradiated at 4.2×10^{-5} dpa. The results are represented in percentage of the 284 FP initially introduced in the simulation box.

another explanation related to the Cu atoms is proposed. These peaks, that we have labelled II''_{Cu} on Fig. 5a, are connected to the stage II peak (like in pure Fe) due to the migration of di-SIAs. As the activation energy for di-interstitial is higher than the activation energy for mono-interstitial, these peaks appear at higher temperatures, compared to peak II for pure Fe, simply because the di-SIAs that formed during the free migration of SIAs are also trapped by Cu atoms and only overcome the trapping in this temperature range, as indicated by the di-SIAs population evolution in Fig. 7.

To conclude on this section on Cu, the higher amplitude observed for the simulated peaks may be attributed, like previously discussed in the pure Fe section, to an over estimation of the recovery.

4.3. AKMC recovery of dilute Fe–Mn alloys

The experimental [14,15] and simulated spectra of the evolution with temperature of the differential isochronal recovery in dilute Fe–Mn alloys are represented in Fig. 8a. They both result from the isochronal annealing, at a rate of 3 K/300 s, of pure Fe and alloys irradiated at 4.2×10^{-5} dpa. The consistency of the results was analysed in the same way described above for Cu.

4.3.1. Stage I

The addition of Mn has a similar influence as Cu on the I_E peak: it disappears when the Mn content of the alloy increases. Another important effect of Mn is the decrease in height of the I_D peak for the highest Mn concentrations in the alloy (1 and 3 at.% Mn alloys).

Maury et al. propose that the suppression of the I_E peak is due to the formation of stable mixed $\langle 1\,1\,0\rangle_{Fe-Mn}$ dumbbells during the migration of the SIAs. The higher the Mn content, the earlier the formation of these mixed $\langle 1\,1\,0\rangle_{Fe-Mn}$ dumbbells. Furthermore, according to the authors, these mixed $\langle 1\,1\,0\rangle_{Fe-Mn}$ dumbbells are more mobile than the SIAs, and as soon as they form, they annihilate with vacancies or form mixed poly-interstitials and particularly mixed di-$\langle 1\,1\,0\rangle_{Fe-Mn}$, which are the only species left above stage I, meaning that no single-interstitial (SIAs or mixed $\langle 1\,1\,0\rangle_{Fe-Mn}$ dumbbells) has survived.

Concerning the decrease of the height of the I_D peak, Maury and co-workers proposed that this can be related to some phase trans-

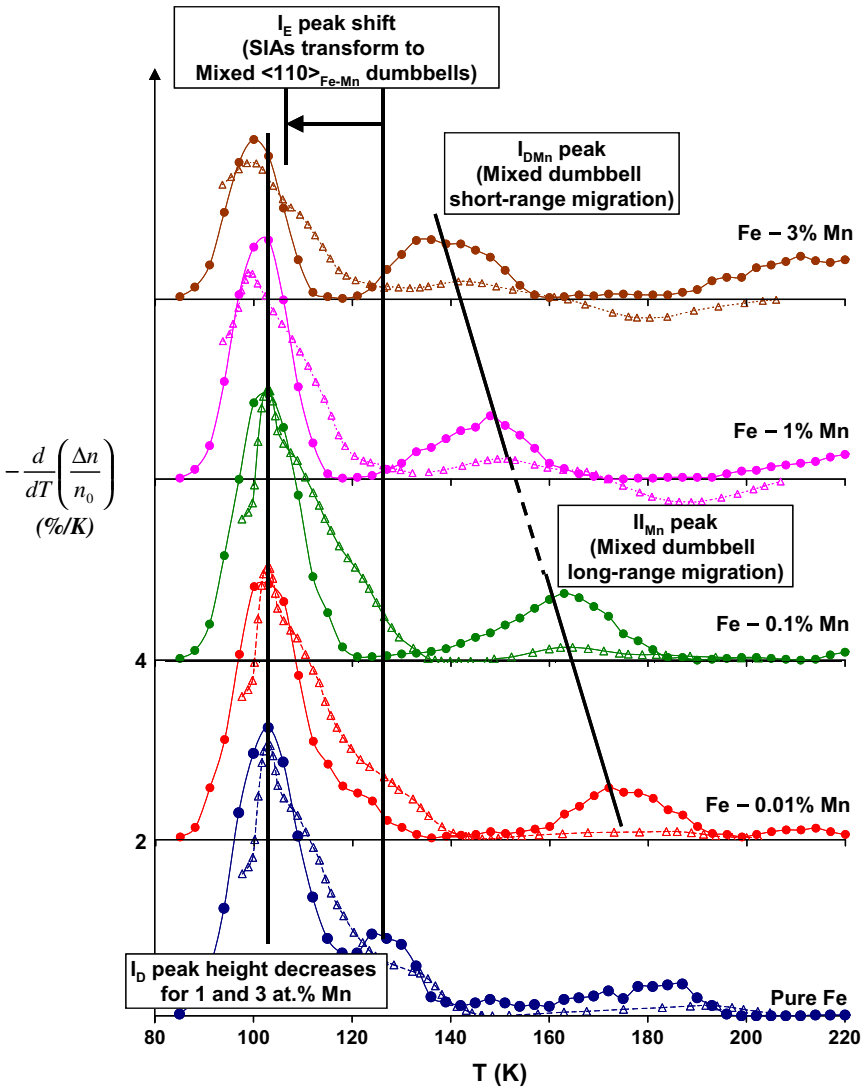

Fig. 8a. Differential isochronal recovery spectra of Fe and Fe–Mn alloys: influence of Mn content. The simulated results (full lines and solid symbols) were obtained for $150 \times 150 \times 150$ (in lattice units) simulation boxes, initially containing 284 FP (corresponding to an initial irradiation dose of 4.2×10^{-4} dpa), that were isochronally annealed at a rate of 3 K/300 s. For comparison, experimental results (dashed lines and open symbols) of Maury et al. [15], obtained for identical conditions, are also shown. An enlargement factor of 3 has been applied to the experimental spectra in (b) to point out the behaviours observed in stage II.

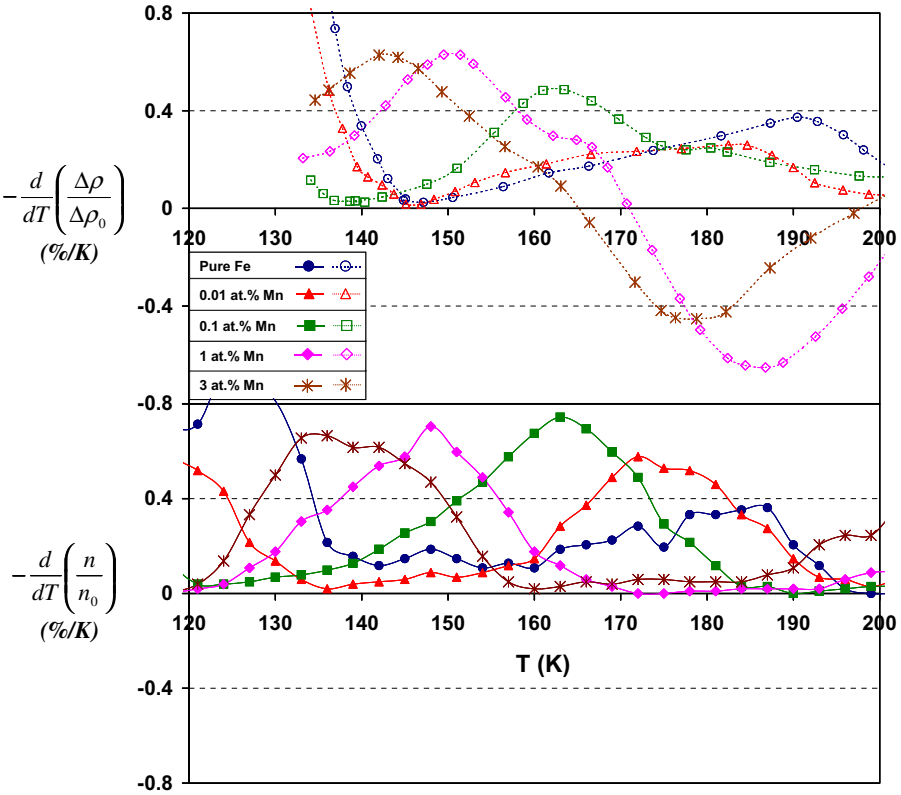

Fig. 8b. Zoom of Fig. 8a.

formations, i.e., to Mn atoms in a crystallographic environment different from the α-phase of the dilute alloys.

Both modifications on I_D and I_E peaks with increasing Mn content have been observed in the simulated spectra. Moreover, *ab initio* calculations [8] do indeed predict that mixed $\langle 1\,1\,0\rangle_{Fe-Mn}$ dumbbells may form and are stable in Fe–Mn alloys. Fig. 9 shows that in the temperature range of stage I_E, more and more mixed $\langle 1\,1\,0\rangle_{Fe-Mn}$ dumbbells appear in the simulation box when the Mn content increases, concurrently with a decrease in the number of pure $\langle 1\,1\,0\rangle_{Fe-Fe}$ SIAs. A slight increase of the value of the binding energy of the mixed $\langle 1\,1\,0\rangle_{Fe-Mn}$ dumbbells from 0.37 to 0.39 eV was enough to insure a good agreement with experimental results as can be seen in Fig. 8a. Another change with respect to the *ab initio* data was the limitation of the trapping possibility of $\langle 1\,1\,0\rangle_{Fe-Fe}$ SIAs by Mn atoms, by lowering the value of $X1nn^{Comp}\_\langle 1\,1\,0\rangle_{Fe-Fe}$ to 0.02 eV instead of the initial *ab initio* value of 0.10 eV. Concerning the I_D peak modification, as our KMC simulations are performed on a rigid lattice, we cannot test the hypothesis of Maury and co-workers that it is due to an $\alpha \rightarrow \gamma$ phase transformation. However, we propose an alternative explanation on the basis of the evolution of the defect population observed in the simulations. At these concentrations (1–3 at.%), the density of Mn atoms is such

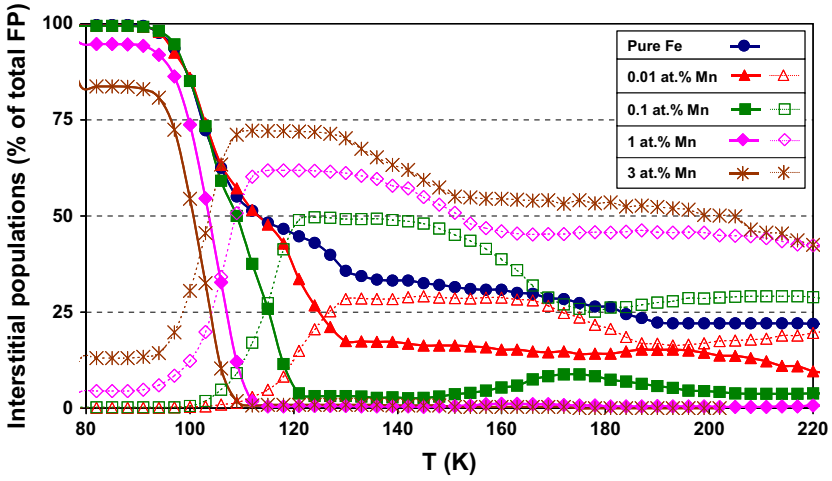

Fig. 9. SIA (full lines and solid symbols) and mixed $\langle 1\,1\,0\rangle_{Fe-Mn}$ dumbbell (dashed lines and open symbols) population evolution with temperature for pure Fe and Fe–Mn alloys isochronally annealed at a rate of 3 K/300 s after being electron-irradiated at 4.2×10^{-5} dpa. The results are represented in percentage of the 284 FP initially introduced in the simulation box.

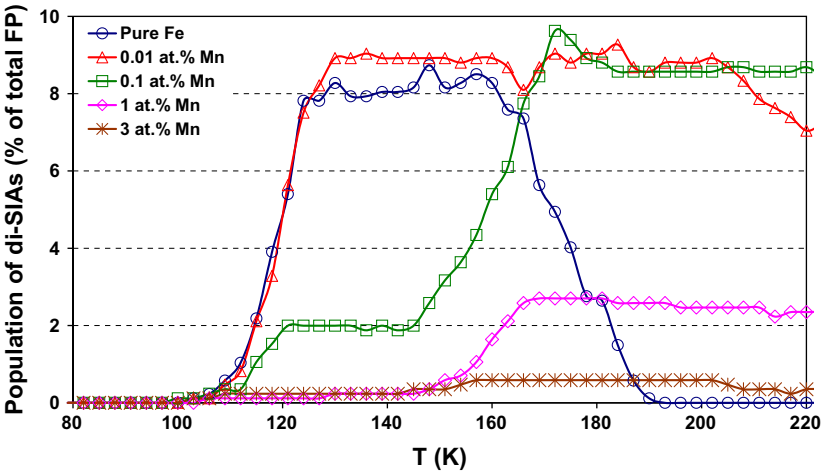

Fig. 10. Di-interstitial defect (di-SIA and/or mixed di-$\langle 1\ 1\ 0\rangle_{Fe-Mn}$ dumbbell) population evolution with temperature for pure Fe and Fe–Mn alloys isochronally annealed at a rate of 3 K/300 s after being electron-irradiated at 4.2×10^{-5} dpa. The results are represented in percentage of the 284 FP initially introduced in the simulation box.

that there is a very high probability for the SIAs to have Mn atoms at the closest neighbouring sites. The probability of correlated recombination is thus lowered since, during their short-range migration, the SIAs have more chances to encounter Mn atoms and form mixed $\langle 1\ 1\ 0\rangle_{Fe-Mn}$ dumbbells in the high content Mn alloys rather than to meet a vacancy. Since the migration energy of these mixed $\langle 1\ 1\ 0\rangle_{Fe-Mn}$ dumbbells is higher than the migration energy of the SIAs, the mixed dumbbells will perform fewer jumps than the SIAs would have done in the same amount of time. Fig. 9 indicates indeed that for the highest Mn content (1 and 3 at.%), all the interstitial-type defects are mixed $\langle 1\ 1\ 0\rangle_{Fe-Mn}$ dumbbells after 110 K.

4.3.2. Stage II

At the scale of Fig. 8a, the observation of the recovery in the temperature range of stage II is not obvious on experimental spectra. An enlargement factor of 3 has therefore been applied to these spectra in Fig. 8b to better highlight the recovery peaks formed.

The experimental spectra show the appearance of a new peak in the temperature range 145–175 K, whose amplitude increases and position shifts to lower temperatures with increasing Mn content. Maury et al. attributed this peak to the migration of di-mixed $\langle 1\ 1\ 0\rangle_{Fe-Mn}$ dumbbells that were formed in stage I. They also observed a stage of negative recovery for the 1 and 3 at.% alloys which, similarly for the case of the I_D peak, they explained by crystallographic phase change issues.

As illustrated in Fig. 8b, a peak with the same features is also visible in the simulated spectra. A good agreement on the temperatures of appearance of this peak with the Mn content is obtained for all the Mn content investigated. This agreement has been obtained after a slight increase of the mixed $\langle 1\ 1\ 0\rangle_{Fe-Mn}$ dumbbell migration energy (from 0.34 eV to 0.38 eV). Nevertheless, a careful examination of the evolution of the defect populations in Figs. 9 and 10 is necessary to provide an interpretation of the experimental spectra based on simulated recovery results. For the 0.01 at.% Mn alloy, the concentration of mixed $\langle 1\ 1\ 0\rangle_{Fe-Mn}$ dumbbells at the end of stage I_E is almost 10% higher than the number of remaining SIAs. We expect therefore the events taking place in stage II for this concentration to be related in majority to single mixed $\langle 1\ 1\ 0\rangle_{Fe-Mn}$ dumbbells and their clusters and only to a smaller extent to SIAs.

For the 0.1 at.% Mn alloy, the proportion of mixed $\langle 1\ 1\ 0\rangle_{Fe-Mn}$ dumbbells is much higher (there are 10 times more mixed $\langle 1\ 1\ 0\rangle_{Fe-Mn}$ dumbbells than SIAs in the simulation box). This suggests that for this concentration, all events are related to mixed $\langle 1\ 1\ 0\rangle_{Fe-Mn}$ dumbbells. For the 1 and 3 at.% Mn alloys, as was stated previously, the formation of mixed $\langle 1\ 1\ 0\rangle_{Fe-Mn}$ dumbbells, which has started very early on (at the beginning of stage I_D), leads to the total disappearance of SIAs. The events occurring in the temperature range (110–200 K) are thus related to mixed $\langle 1\ 1\ 0\rangle_{Fe-Mn}$ dumbbells and/or eventually their clusters as these are the only types of defects present in the simulation box.

At this point, we have identified several events that can occur in stage II, depending on the concentration of the alloy: migration of SIAs or di-SIAs for pure Fe and dilute Mn alloy (typically the 0.01 at.% Mn), formation and migration of mixed $\langle 1\ 1\ 0\rangle_{Fe-Mn}$ dumbbells or their clusters already observed to a smaller extent in dilute alloy, and exclusively in more concentrated alloys (typically from 0.1 at.% Mn).

The recovery spectrum of pure Fe has been previously discussed. The peak observed around 185 K (190 K on the experimental spectrum) is related to the migration of di-SIAs formed during SIAs migration at stage I_E.

The recovery spectra of the dilute alloys exhibit a single peak. As stated previously, according to Fig. 9, this peak is most likely related to the motion of mixed $\langle 1\ 1\ 0\rangle_{Fe-Mn}$ dumbbells principally, against the interpretation of Maury and co-workers. The interpretation of these authors is that mixed $\langle 1\ 1\ 0\rangle_{Fe-Mn}$ dumbbells recombine with vacancies or aggregate as clusters as soon as they form, which means that stage II peak is due to mixed $\langle 1\ 1\ 0\rangle_{Fe-Mn}$ dumbbells clusters exclusively. Furthermore in our analysis, we show that this peak corresponds to two kinds of events depending on the distance travelled by the mixed $\langle 1\ 1\ 0\rangle_{Fe-Mn}$ dumbbells. For the 0.01 at.% Mn and 0.1 at.% Mn alloys, the peak, that we denoted II_{Mn} in Fig. 8a, stems from the long-range migration of the mixed $\langle 1\ 1\ 0\rangle_{Fe-Mn}$ dumbbells. We attribute the shift observed to a decreasing "effective" migration energy with increasing concentration of mixed dumbbells in the alloy.

For the 1 and 3 at.% Mn alloys, the concentration of the mixed dumbbells at the end of I_E is so large that the "effective" energy necessary for their motion becomes very low and the probability of finding a vacancy at neighbouring sites is very high, which results in a shortening of the trajectory before recombination. The resulting peak has therefore been labelled I_{DMn} as we can attribute it to the short-range migration of the mixed $\langle 1\ 1\ 0\rangle_{Fe-Mn}$ dumbbells.

To conclude on this section on Mn alloys, the simulation results highlight a good qualitative reproduction of the experimental

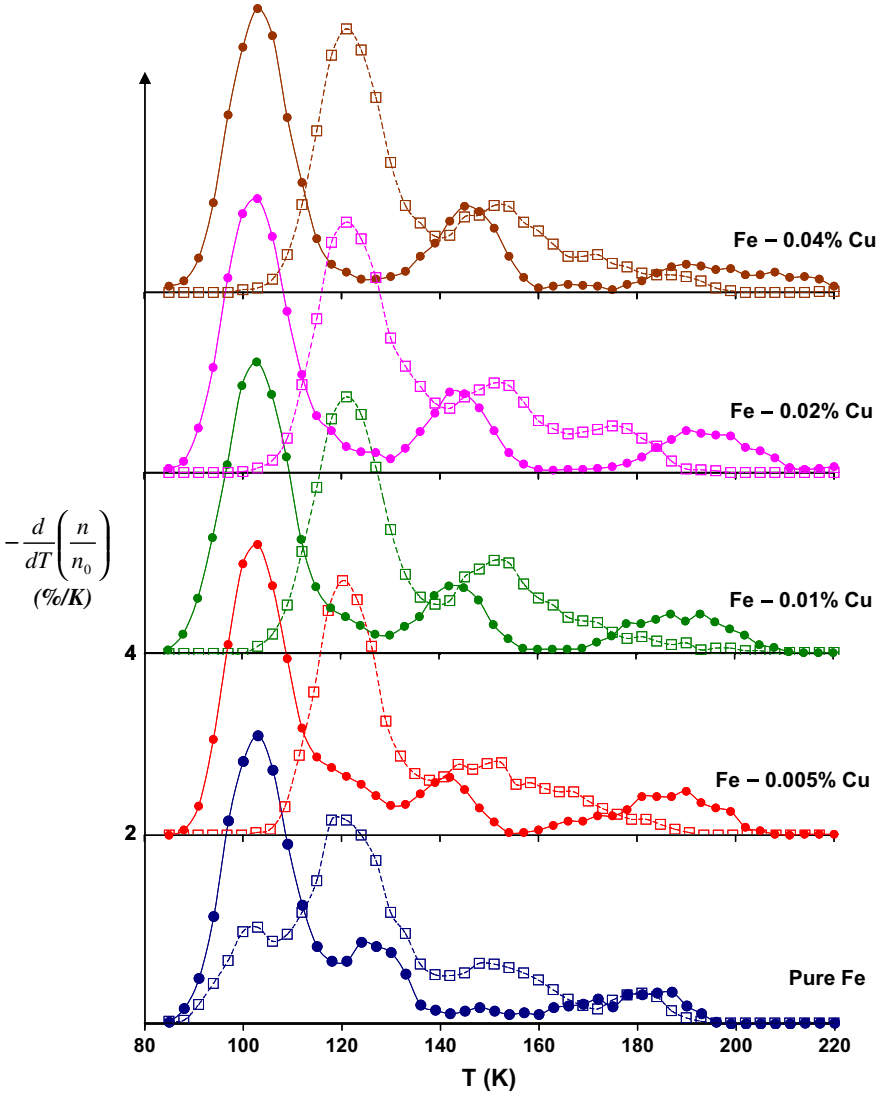

Fig. 11. Differential isochronal recovery spectra of Fe and Fe–Cu alloys: influence of Cu content. The simulated results were obtained for 150 × 150 × 150 (in lattice units) simulation boxes, initially containing 284 FP (corresponding to an initial irradiation dose of 4.2×10^{-5} dpa), which were isochronally annealed at a rate of 3 K/300 s. Spectra in full lines and solid symbols were obtained after adjustment; whereas spectra obtained with the raw *ab initio* data are represented in dashed lines and open symbols.

spectra, despite some quantitative differences already observed and discussed in the pure Fe and Cu alloys sections. We have also shown that it is possible to provide new tentative interpretations of the experimental observations. The model needs however to be further tested on simple irradiation cases.

4.4. Concluding remarks on the adjustment procedure

From the discussions presented in the previous three sections, we note that the parameterization of the AKMC model to reproduce experimental isochronal annealing results has been achieved trough the adjustment of some of the raw *ab initio* data in the model. These data are: the SIA migration energy, the di-SIA migration energy trough the adjustment of the 1st and 2nd nearest neighbour interaction energies of the two dumbbells, and finally the solute-dumbbell migration and interaction energies as summarized in Table 1. The adjustment concerns a total of eight *ab initio* data over the 15 involved: three for pure Fe, one for Fe–Cu, and four for Fe–Mn. The adjustment method was based on modifications, within the inherent ±0.1 eV range of uncertainty for *ab initio* calculations, that only preserve the original character of the data adjusted. The resulting changes range from 80% reduction (0.10 eV changed into 0.02 eV) to 86% increment (0.07 eV changed into 0.13 eV) of the original values, but this result has to be taken with caution for two main reasons: these uttermost changes concern only two data over the eight (the major changes ranging from 20% reduction to 5% increment) and the small values of the quantity involved explain the "large" impact caused by any change. Indeed going from 0.10 eV to 0.02 eV corresponds to a decrease of 0.08 eV only. Besides these quantitative aspects, we would like to emphasize how necessary the data adjustment was, and this is illustrated in Fig. 11. This figure presents, in the case of isochronal annealing simulations of Fe–Cu alloys, results obtained before (i.e., with the raw *ab initio* data) and after the adjustment. It shows the significant differences on the temperature of appearance as well as the behaviour of all the recovery peaks.

5. Conclusions

We have shown how *ab initio* based KMC simulations can realistically mimic isochronal resistivity recovery experiments of electron-irradiated materials considering simple but motivated

assumptions and using limited input parameters. The materials here considered were pure Fe and dilute Fe–Cu and Fe–Mn alloys. The model parameters were based on *ab initio* predictions, but had to be readjusted slightly to better reproduce the results of resistivity recovery experiments on similar materials and for similar conditions. The experimental results of Takaki et al. [13] for pure Fe and Maury et al. [14,15] for Fe–Cu and Fe–Mn alloys were used for comparison.

The resulting model describes qualitatively well the experimentally observed behaviour under isochronal annealing and allows for precise interpretations of the defect–solute interactions and defect activation energies. Most of the previous experimental interpretations of the recovery spectra were verified and confirmed. In the cases where *ab initio* predictions of simulated results were in disagreement with the interpretations in the literature, the here proposed model has been used to identify, with access to atomic detail, new interpretations of the mechanisms involved:

(i) Contrary to Maury and co-workers, we do not expect the formation of any stable mixed $\langle 1\,1\,0\rangle_{Fe-Cu}$ dumbbells in Fe–Cu alloys. The efficient trapping of SIAs by Cu atoms is enough to account for the behaviour observed in the spectra.
(ii) The peak in Fe–Cu observed in the temperature range 170–200 K is not due to residual impurities but stems from the migration of di-SIAs previously trapped by Cu atoms.
(iii) We have been able to observe in the Fe–Mn spectra the decrease in height of the I_D peak for higher Mn content, which we relate to an earlier transformation of SIAs to mixed $\langle 1\,1\,0\rangle_{Fe-Mn}$ dumbbells, instead of the crystallographic issues proposed by Maury and co-workers.
(iv) Contrary to these authors, we expect the behaviour observed in the temperature range of stage II in Fe–Mn to be essentially due to single-interstitial defects (SIAs and/or mixed $\langle 1\,1\,0\rangle_{Fe-Mn}$ dumbbells) and not exclusively mixed poly-interstitials.

On the other side, although the model is very satisfactory in reproducing qualitatively experimental recovery results, some limitations still remain. Nonetheless, we believe that these limitations are not strong enough to prevent the validation of this AKMC model which can now be used with confidence for simulations of medium term evolution of the microstructure under irradiation, such as the irradiation induced and/or accelerated precipitation of Cu and Mn in bcc Fe.

Acknowledgements

This work has been performed within the European PERFECT project (FI6O-CT-2003-508840) and has been partially financed by the European Commission FP7 project PERFORM-60, under grant agreement number 232612. This work is also a part of the research program of the EDF-CNRS joint laboratory EV2VM (Study and Modelling of the Microstructure for Ageing of Materials).

References

[1] J.T. Buswell, W.J. Phythian, R.J. McElroy, S. Dumbill, P.H.N. Ray, J. Mace, R.N. Sinclair, J. Nucl. Mater. 225 (1995) 196.
[2] P. Auger, P. Pareige, S. Welzel, J.-C. Van Duysen, J. Nucl. Mater. 280 (2000) 331.
[3] E. Vincent, C.S. Becquart, C. Domain, J. Nucl. Mater. 351 (2006) 88.
[4] E. Vincent, C.S. Becquart, C. Domain, Nucl. Inst. Meth. Phys. Res. B 255 (2007) 78.
[5] C. Domain, C.S. Becquart, J.C. Van Duysen, Mater. Res. Soc. Symp. Proc. 650 (2001) R3.25.1.
[6] E. Vincent, C.S. Becquart, C. Domain, J. Nucl. Mater. 382 (2008) 154.
[7] E. Vincent, C.S. Becquart, C. Domain, J. Nucl. Mater. 359 (2006) 227.
[8] E. Vincent, C.S. Becquart, C. Domain, Nucl. Inst. Meth. Phys. Res. B 228 (2005) 137.
[9] W.M. Young, E.W. Elcock, Proc. Phys. Soc. 89 (1966) 735.
[10] C.-C. Fu, F. Willaime, P. Ordejón, Phys. Rev. Lett. 92 (2004) 175503.
[11] C.S. Becquart, C. Domain, Nucl. Inst. Meth. Phys. Res. 202 (2003) 44.
[12] E. Vincent, C.S. Becquart, C. Pareige, P. Pareige, C. Domain, J. Nucl. Mater. 373 (2008) 387.
[13] S. Takaki, J. Fuss, H. Kugler, U. Dedek, H. Schultz, Radiat. Eff. 79 (1983) 87.
[14] F. Maury, A. Lucasson, P. Lucasson, P. Moser, Y. Loreaux, J. Phys. F16 (1986) 523.
[15] F. Maury, A. Lucasson, P. Lucasson, P. Moser, F. Faudot, J. Phys. Condens. Matter 2 (1990) 9291.
[16] F. Maury, A. Lucasson, P. Lucasson, P. Moser, Y. Loreaux, J. Phys. F: Met. Phys. 15 (1985) 1465.
[17] H. Abe, E. Kuramoto, J. Nucl. Mater. 271–272 (1999) 209.
[18] R.R. Hasiguti, Nucl. Metall. 18 (1973) 1.
[19] H.J. Blythe, H. Kronmüller, A. Seeger, F. Walz, Phys. Status Solidi (a) 181 (2000) 233.
[20] P. Olsson, J. Nucl. Mater. 386–388 C (2009) 86.
[21] C. Domain, C.S. Becquart, Phys. Rev. B 65 (2001) 024103.